IEEE Photonics Journal
An IEEE Photonics Society Publication

Ultracompact Phase Modulator Based on a Cascade of NEMS-Operated Slot Waveguides Fabricated in Silicon-on-Insulator

Volume 4, Number 3, June 2012

K. Van Acoleyen, Student Member, IEEE
J. Roels
P. Mechet, Student Member, IEEE
T. Claes, Student Member, IEEE
D. Van Thourhout, Member, IEEE
R. Baets, Fellow, IEEE

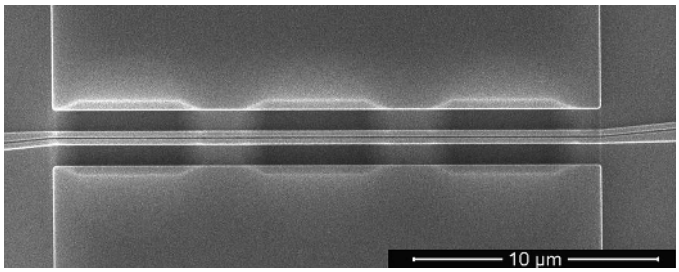

DOI: 10.1109/JPHOT.2012.2198880
1943-0655/$31.00 ©2012 IEEE

IEEE photonics SOCIETY

IEEE

Ultracompact Phase Modulator Based on a Cascade of NEMS-Operated Slot Waveguides Fabricated in Silicon-on-Insulator

K. Van Acoleyen, *Student Member, IEEE*, J. Roels, P. Mechet, *Student Member, IEEE*, T. Claes, *Student Member, IEEE*, D. Van Thourhout, *Member, IEEE*, and R. Baets, *Fellow, IEEE*

Photonics Research Group, Department of Information Technology (INTEC), Ghent University-imec, 9000 Ghent, Belgium
Center for Nano- and Biophotonics (NB-Photonics), Ghent University, 9000 Ghent, Belgium

DOI: 10.1109/JPHOT.2012.2198880
1943-0655/$31.00 ©2012 IEEE

Manuscript received April 26, 2012; accepted May 4, 2012. Date of current version May 15, 2012. This work was supported by the Methusalem project Smart Photonic ICs of Ghent University and the IAP project Photonics@be. Corresponding author: K. Van Acoleyen (e-mail: karel.vanacoleyen@intec.ugent.be).

Abstract: Phase modulation is one of the key functionalities in an integrated photonics circuit. In the silicon photonics platform, several approaches have been undertaken. The thermooptic effect is slow and relatively power hungry, whereas a carrier-based approach is fast ($>$ Gb/s) but lossy and weak. Integration of other (e.g., electrooptic) materials typically struggles with fabrication issues that limit the effect. Here, we present a nanoelectromechanical systems-based approach. By applying a voltage over a freestanding slot waveguide, the slot width will change, resulting in an effective index change and thus a phase change. Using a cascaded structure, the effect can be enlarged without reducing the speed. A phase change of 40° was observed for a voltage of 13 V over a cascade of three 5.8-μm-long freestanding slots. The expected speed is in the MHz range.

Index Terms: Silicon nanophotonics, micro and nano optoelectromechanical systems (MOEMS), waveguide devices.

1. Introduction

Optical phase modulation is of key importance in data modulation or tuning applications. Integrated photonics has received a lot of attention in this area due to the possibility to fabricate low-power, compact phase modulators. One of these platforms is the silicon photonics platform. Using complementary metal–oxide–semiconductor (CMOS) compatible processes, very compact photonic structures such as integrated waveguides, wavelength (de)multiplexers, interferometers, sensors or optical filters can be fabricated.

Several approaches can be taken to integrate a phase modulator in this platform. The easiest and simplest approach of phase modulation is using the thermooptic effect in silicon. While it is a large effect, it also has a relatively large power consumption due the continuous current flow. Furthermore, the speed is limited as the thermooptic response is in the μs range. This effect has been used to e.g., tune the resonance frequency of a ring resonator [1], [2]. Carrier-based modulators are capable to reach up to several tens of Gb/s and higher, but are relatively large and lossy as the carriers increase the optical absorption of the waveguides [3], [4]. Here, we present a compact,

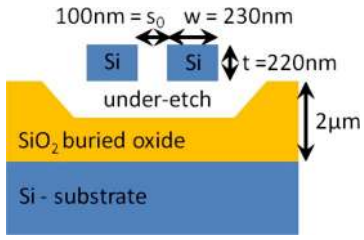

Fig. 1. Cross section of an underetched slot waveguide on silicon-on-insulator.

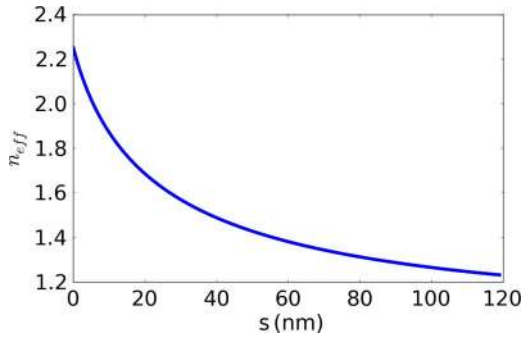

Fig. 2. Effective index of the fundamental TE-like mode of the slot as a function of slot width at a wavelength of 1550 nm.

low-power optical phase modulation technique based on nanoelectromechanical systems (NEMS) using an underetched slot waveguide.

Apart from its attractive optical properties, crystalline silicon also has good mechanical properties. This stimulated a rapid development of the NEMS field in e.g., fabricating ultrasensitive sensors [5]. This platform furthermore allowed to observe and measure optical forces on integrated photonic circuits [6]–[8]. The principle of using a freestanding slot waveguide as phase modulator was already explained in [9]. A first proof-of-principle component using one single underetched region was presented in [10]. Here, we present a cascaded structure and investigate the dynamic behavior in more detail.

As a mechanical motion can induce a large effective index shift, compared to other techniques such as heating, carrier injection/depletion, electrooptic effect, . . . we can have an ultrasmall phase tuner. Such a structure works capacitively meaning that only power will be consumed when switching. The speed will depend on the mechanical relaxation constant of the structure, which lies in the MHz range for a typical freestanding waveguide. Since the structure discussed here was not optimized for high-speed operation, large distributed RC constants are present limiting the speed.

In the next section, the working principle of the slot waveguide is explained. Section 3 gives a mathematical description together with some simulation results. Section 4 presents the device layout and fabrication, followed by the measurement setup and results in Section 5. A conclusion is finally formulated in Section 6.

2. Principle

The principle of phase modulation is based on the fact that the effective index of a slot waveguide will change by changing the slot width. The effective index of the fundamental TE-like mode of the slot waveguide (Fig. 1) as a function of the slot width *s* was calculated using the Fimmwave mode solver [11] and can be found in Fig. 2. A large change in effective index occurs as the slot width becomes smaller. The slot width can be changed by underetching the slot waveguide and applying a voltage. The structure can then be considered as a capacitor. By applying a voltage across the

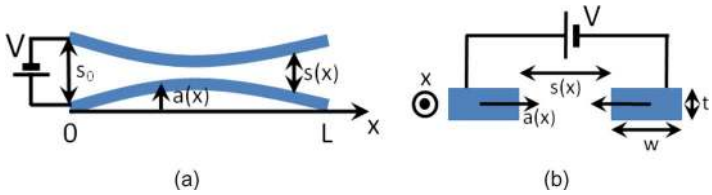

Fig. 3. Mathematical description of the slot waveguide-based phase modulator: (a) top view, (b) cross-sectional view.

slot, it is well known that the beams (plates of a charged capacitor) will attract each other. By increasing the voltage, the beams are attracted and the slot width becomes smaller. This increases the attractive force even more. At a certain point, the attractive force becomes too large for the slot to be countered by the elastic force and the system becomes unstable resulting in a collapse of the slot waveguide. This is known as the "pull-in" effect in the microelectromechanical systems (MEMS) world and as a general rule of thumb occurs when the slot deviation is larger than one third of the nominal width.

3. Mathematical Description

Fig. 3 shows a top view and cross-sectional view of the slot waveguide in which all the variables introduced below are denoted. The movement $a(x)$ of the beams of the slot can be described by the Euler beam equation, where the residual axial stress is neglected in first instance

$$EI\frac{d^4a}{dx^4} = p(x) \tag{1}$$

where E is Young's modulus $(= 169$ GPa in Si for the crystallographic direction of interest), $p(x)$ is the force distribution along the beam and I is the beam's area moment of inertia. In the direction of interest I is defined as

$$I = \frac{tw^3}{12} \tag{2}$$

with w and t the width and thickness of the beam, respectively. When a voltage is applied across the slot, a force will be exerted on both beams which will depend on the width of the slot waveguide. The force distribution $p(x)$ (N/m) can be expressed as

$$p(x) = \frac{1}{2}V^2\frac{\partial C[s(x)]}{\partial s(x)} \tag{3}$$

where V is the applied voltage and $C[s(x)]$ is the capacitance distribution (F/m) across the slot, which is a function of $s(x)$, the width of the slot. The capacitance distribution is given by

$$C[s(x)] = \epsilon_0\frac{t}{s(x)}. \tag{4}$$

The magnitude of the force distribution is then given by

$$p(x) = \frac{1}{2}V^2\frac{\epsilon_0 t}{s(x)^2} \tag{5}$$

with ϵ_0 the vacuum permittivity. There is a squared dependence on the applied voltage and an inverse squared dependence on the slot width. This width between the slots is dependent on the beam excursion $a(x)$ as

$$s(x) = s_0 - 2a(x) \tag{6}$$

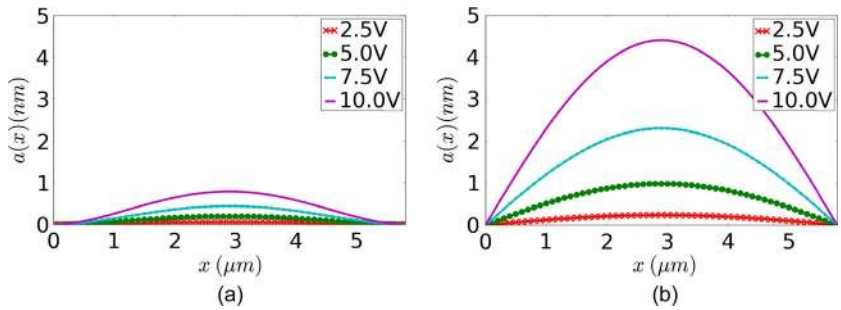

Fig. 4. Beam excursion of one of the beams as a function of x for different applied voltages: (a) fixed boundary conditions, (b) hinged boundary conditions.

where s_0 is the slot width when no voltage is applied. Inserting (6) in (5) and (5) in (1), we get the following nonlinear differential equation:

$$EI\frac{d^4a}{dx^4} = \frac{1}{2}V^2\frac{\epsilon_0 t}{[s_0 - 2a(x)]^2}. \tag{7}$$

Different boundary conditions can be used. Fixed boundary conditions at the clamping points $x = 0$ and $x = L$ allow no displacement or rotation

$$a = 0; \qquad \frac{da}{dx} = 0. \tag{8}$$

Hinged boundary conditions allow no displacement, but do allow rotation at the clamping points. The boundary conditions become

$$a = 0; \qquad \frac{d^2a}{dx^2} = 0. \tag{9}$$

Let us look at an example. We take a length of $L = 5.8$ μm (which is the beam length used in the fabricated device). Equation (7) is solved numerically using the parameters given in Fig. 1. In Fig. 4, the beam excursion of one of the slot beams with a length of $L = 5.8$ μm is shown as a function of x for different voltages, when fixed or hinged boundary conditions are used. When the voltage becomes larger than the "pull-in" voltage, the system becomes unstable and no solution is found. For $L = 5.8$ μm, the pull-in voltage was determined to be around 34 V for fixed and 15 V for hinged boundary conditions. The figure shows that the beam excursion is very dependent on the used boundary conditions.

When the beam excursion is known, the phase change can be calculated as

$$\Delta\phi = \frac{2\pi}{\lambda}\int_0^L n_{eff}[s_0 - 2a(x)]\,dx \tag{10}$$

with λ the wavelength of light and $n_{eff}[s(x)]$ is given by Fig. 2. The predicted phase change for $L = 5.8$ μm is given in Fig. 5. The maximum effect is the same for both cases as the pull-in effect occurs at the same beam deviation. The needed voltage for fixed boundary conditions is, however, much higher than for hinged boundary conditions.

The length of the beam has a large influence on the effect. Fig. 6 shows the phase change as a function of applied voltage for different lengths of the beams for fixed boundary conditions. The phase change increases more sharply for larger voltages up to the point where "pull-in" occurs. One can see that for longer beams, the effect becomes large for a small voltage.

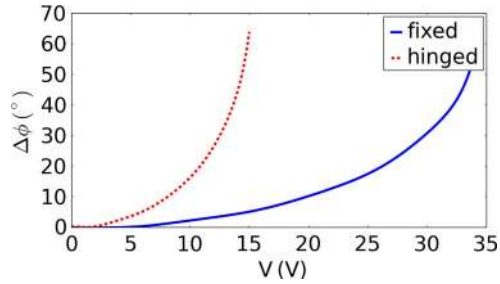

Fig. 5. Theoretically predicted phase change as a function of applied voltage across the slot with $L = 5.8$ μm for fixed and hinged boundary conditions.

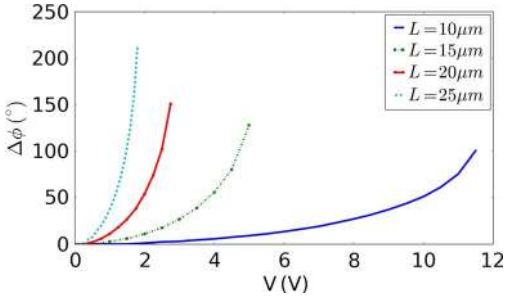

Fig. 6. Theoretically predicted phase change as a function of applied voltage across the slot for different lengths L for fixed boundary conditions. The curves are drawn up to the point where "pull-in" occurs.

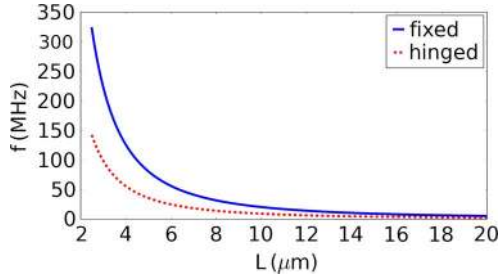

Fig. 7. Fundamental mechanical resonance frequency of one of the slot beams as a function of length L.

While the effect becomes larger for longer beams, so does the mechanical relaxation time. The speed of the system is limited by the mechanical resonance frequency of the beams. The fundamental resonance frequency f_0 of such a beam is given by

$$f_0 = \frac{1}{2\pi}\frac{p^2}{L^2}\sqrt{\frac{EI}{\rho S}} \tag{11}$$

with L the length of the beam, I the moment of inertia given by (2), E Young's modulus, ρ the mass density of silicon ($\rho = 2.3290$ g $\cdot$ cm^{-3}) and S the beam cross section. The parameter $p = 4.730$ for fixed boundary conditions and $p = \pi$ for hinged boundary conditions. Note the inverse L^2 dependence, meaning that using a shorter beam results in an increase of the resonant frequency. Fig. 7 shows the fundamental mechanical resonant frequency as a function of beam length. A speed of several tens of MHz can be obtained by using short freestanding structures. To get a large effect while keeping a high speed a cascade of short underetched structures is used as is discussed in Section 5.

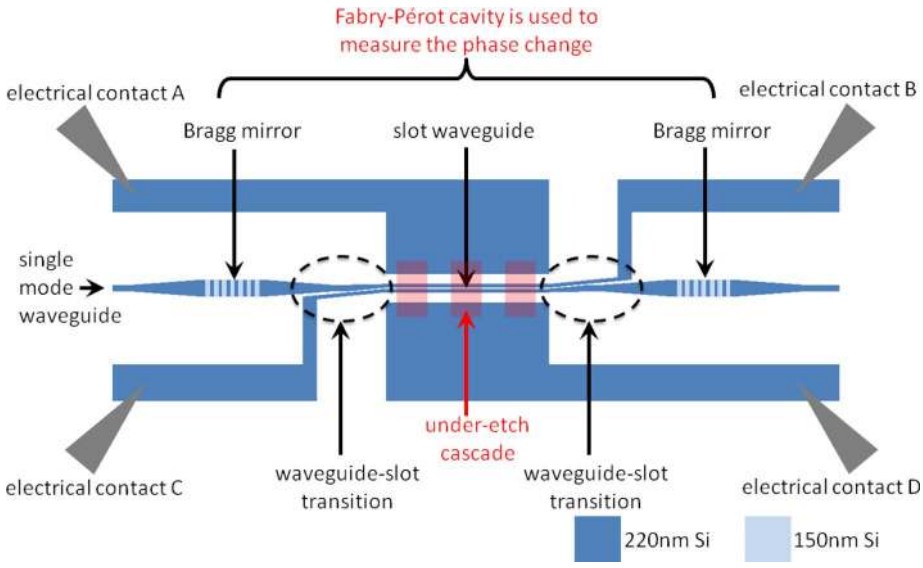

Fig. 8. Schematic layout of the NEMS-based phase modulator.

4. Device Layout and Fabrication

Fig. 8 shows a schematic layout of the fabricated phase modulator. It was fabricated with 193 nm deep-ultraviolet (UV) lithography using a standardized process flow with CMOS compatible processes at *imec* through ePIXfab [12]. An silicon-on-insulator (SOI) wafer with a 2 μm buried oxide and a 220 nm top silicon layer is used. An etch step of 220 nm then defines the waveguides and slot waveguide while a 70 nm etch allows us to create shallow gratings, used for the Fabry–Pérot cavity and fiber grating couplers [13]. The Fabry–Pérot cavity allows us to measure the phase change by means of a spectral shift of the resonant wavelengths of the cavity. A cross section of the slot and all the designed dimensions is shown in Fig. 1. The slot width is 100 nm wide, while the slot beams are 230 nm wide.

Light enters through a single mode waveguide and is then guided to the slot waveguide through a specially designed transition [14]. The slot waveguide is underetched so that part of the slot is freestanding. After passing through this underetched slot, light is guided back to a single mode waveguide. The transitions are designed so that a voltage can be placed across the slot beams by using the electrical contacts B and C. The whole structure is placed between two Bragg mirrors that form the Fabry–Pérot cavity. These Bragg mirrors were fabricated in a wide waveguide as the effective index of a wide waveguide is independent of the waveguide width making the mirror reflection less dependent on fabrication deviations.

The structure is underetched by defining three etch regions of 3 μm length using contact-mask lithography and etching the buried oxide with buffered hydrofluoric acid (HF) for about 6 to 8 min. As the beams are relatively short, we were able to overcome the stiction problems that arise through capillary forces without the need of critical point drying. Fig. 9 shows a scanning electron microscope (SEM) picture of the phase modulator using a cascade of three freestanding underetched regions. Due to the isotropic HF etching, the underetched length is increased to 5.8 μm.

5. Measurements

5.1. Setup

Fig. 10 shows a schematic of the measurement setup. The structure is excited through the broadband output light of a superluminescent light emitting diode (SLED). The light first goes through a polarization controller to rotate the light to the TE-like mode of the waveguide. It is then

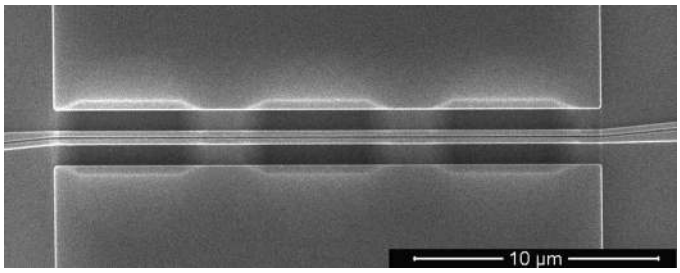

Fig. 9. SEM picture of the fabricated NEMS-based phase modulator using a cascade of short underetched regions.

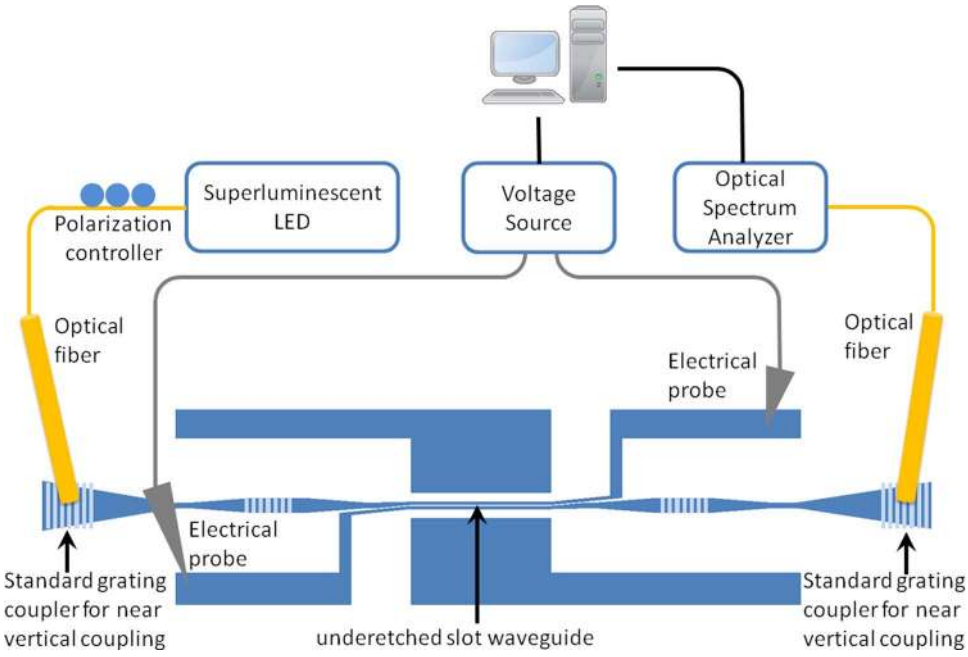

Fig. 10. Measurement setup for the characterization of the NEMS-based phase modulator: broadband light from an SLED goes through a polarization controller and is coupled into the photonic circuit using a grating coupler. The light at the output is sent to an Optical Spectrum Analyzer (OSA). A voltage source is connected to the Si-pads to apply a voltage over the slot.

coupled in an integrated waveguide using a standard grating coupler for near-vertical coupling [15] and passes through the Fabry–Pérot cavity in which the slot waveguide is located. The output of the cavity is then sent to an OSA to detect peak shifting as a result of the phase change in the cavity. A voltage source is connected to the silicon pads to contact the waveguides.

5.2. Results

The measured spectra for the modulator are shown in Fig. 11. The weak Bragg mirrors and losses in the cavity result in broad resonances. For larger wavelengths, the transmission decreases which suggests that the slot mode is reaching cutoff at the non underetched region (since there is no cutoff frequency when a slot is underetched).

By measuring the peak shift for different voltages, the effective phase change inside the slot can be calculated. This is shown in Fig. 12, where also the theoretical solution is shown for different applied boundary conditions. A phase-change of about 40° was demonstrated for an applied voltage of 13 V. It is clear that the measurement results lie in between these two extremes. We also

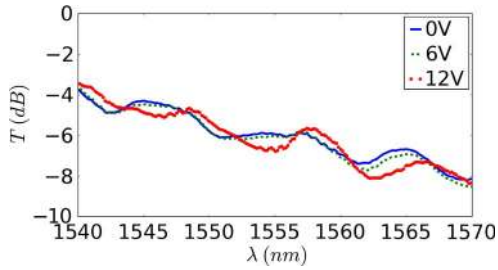

Fig. 11. Measured spectra of the phase modulator consisting of a cascade of three 5.8 μm long underetched regions for different applied voltages.

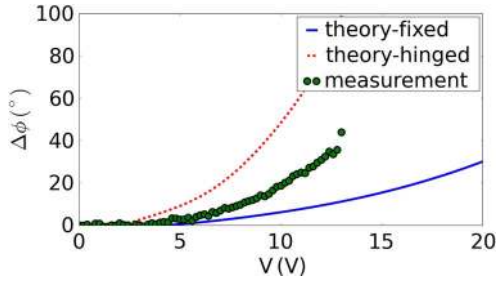

Fig. 12. Theoretically predicted and measured phase change as a function of applied voltage across the cascade of three 5.8 μm underetched slots.

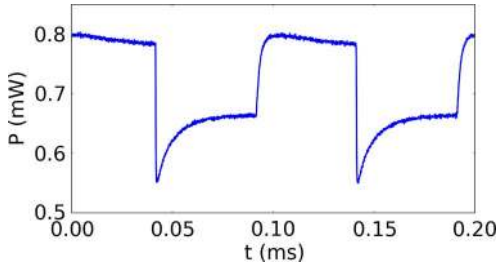

Fig. 13. Measured dynamic behavior of the slot waveguide-based phase modulator.

note that the theoretical phase change is very dependent on the actual underetch length (see Fig. 6) and the initial slot width s_0. When s_0 becomes smaller, the change in effective index becomes larger which can be concluded from Fig. 2. By increasing number of elements in the cascade, a π phase shift can easily be obtained.

The speed of the cascade is predicted to be faster than the speed of a longer single underetched slot because of the higher fundamental mechanical resonance frequency given in Fig. 7. The fundamental resonance frequency of a 5.8 μm beam is 60 MHz and 26 MHz for fixed and hinged boundary conditions, respectively. To investigate the dynamic behavior, a square wave is applied across the cascade. We excite the modulator with a single wavelength and as the Fabry–Pérot resonance will shift (as seen in Fig. 11), the measured optical power will vary. This signal is then amplified with and erbium-doped fiber amplifier (EDFA), passes through a wavelength filter to filter out the broadband EDFA noise gain and is then measured with a high-speed photodiode. Fifty spectra are then averaged to reduce the noise, as we are measuring small power variations.

Fig. 13 shows the measurement result. One of the beams is kept at ground while the other beam will have a square signal of 10 V and 100 μs period. The substrate is also grounded so that the

beams are not only attracted to each other, but one beam is also attracted toward the substrate. This force is, however, an order of magnitude smaller as the distance to the substrate is 2 μm, compared to the 100 nm slot spacing. This asymmetric attraction can be overcome by using a bipolar source (one beam at $+5$ V and the other beam at -5 V) as both beams will then be attracted toward each other and also to the substrate.

The initial drop in power appears when the voltage is switched on at one beam from 0 to 10 V. The reaction of the beam can be described by a simple damped oscillator. The beam is excited with a step response when the square wave is applied and thus multiple mechanical resonance frequencies will be excited. These will however be damped due to losses. There are three sources of losses that will damp the oscillations: intrinsic losses due to defects, clamping losses and gas damping. The gas damping will be the limiting loss factor which will limit the Q factor of the mechanical resonance and can be described by [16]

$$Q_{\text{gas}} = \frac{m_{eff}\omega_0\sqrt{k_B T/m}}{pS} \tag{12}$$

with m_{eff} the effective mass of the beam, ω_0 the angular frequency of oscillation, k_B Boltzmann's constant, T the temperature, m the individual molecule mass, p the gas pressure and S the surface area of the resonator. For air damping, this results in a Q_{gas} of only 7 for a 5.8 μm beam at atmospheric pressure for the fundamental resonance frequency using fixed boundary conditions. The damping time is then $2Q/\omega_0 = 37$ ns limiting the effect to a few tens of MHz.

The structure was, however, not optimized for high-speed operation. There was no high-speed electrical pad layout, limiting the measurement speed to a few MHz. Furthermore, the complete structure $(\text{slot} + \text{silicon pad} + \text{access waveguides})$ also acts as a large distributed capacitance to the substrate and has a high distributed resistance. The complete resistance is of the order 20 MΩ while the complete capacitance is of the order 0.35 pF. The exact dynamic behavior is then difficult to predict. The RC constant is of the order 7 μs which explains the slow exponential effects visible in Fig. 13. The initial response is however as fast as we were able to measure showing that the structure can operate in the MHz range.

6. Conclusion

A novel type of phase modulation was investigated using a NEMS-based approach. Applying a voltage over the two beams of an underetched slot waveguide changes the beam position and thus its effective index. As this is a capacitive structure, power is only dissipated when switching. By using a cascade of short underetched slot waveguides, the effect can be large while maintaining high-speed operation. The expected speed is in the MHz range. For a cascaded structure of three 5.8 μm long freestanding slot waveguides, a phase change of 40° was measured for a voltage of 13 V.

Acknowledgment

K. Van Acoleyen acknowledges the Research Foundation—Flanders (FWO) for a research grant. The authors would like to thank B. De Geyter for the help in the design of the component and E. Hallynck, L. Van Landschoot, and S. Verstuyft for the help with the postprocessing.

References

[1] R. L. Espinola, M. C. Tsai, J. T. Yardley, and R. M. Osgood, "Fast and low-power thermooptic switch on thin silicon-on-insulator," *IEEE Photon. Technol. Lett.*, vol. 15, no. 10, pp. 1366–1368, Oct. 2003.
[2] J. Van Campenhout, W. M. J. Green, S. Assefa, and Y. A. Vlasov, "Integrated NiSi waveguide heaters for CMOS-compatible silicon thermo-optic devices," *Opt. Lett.*, vol. 35, no. 7, pp. 1013–1015, Apr. 2010.
[3] G. T. Reed, G. Mashanovich, F. Y. Gardes, and D. J. Thomson, "Silicon optical modulators," *Nat. Photon.*, vol. 4, no. 8, pp. 518–526, Aug. 2010.
[4] D. J. Thomson, F. Y. Gardes, J.-M. Fedeli, S. Zlatanovic, Y. Hu, B. P. P. Kuo, E. Myslivets, N. Alic, S. Radic, G. Z. Mashanovich, and G. T. Reed, "50-Gb/s silicon optical modulator," *IEEE Photon. Technol. Lett.*, vol. 24, no. 4, pp. 234–236, Feb. 2012.

[5] I. De Vlaminck, J. Roels, D. Taillaert, D. Van Thourhout, R. Baets, L. Lagae, and G. Borghs, "Detection of nano-mechanical motion by evanescent light wave coupling," *Appl. Phys. Lett.*, vol. 90, no. 23, pp. 233116-1–233116-3, Jun. 2007.
[6] J. Roels, I. De Vlaminck, L. Lagae, B. Maes, D. Van Thourhout, and R. Baets, "Tunable optical forces between nanophotonic waveguides," *Nat. Nanotechnol.*, vol. 4, no. 8, pp. 510–513, 2009.
[7] D. Van Thourhout and J. Roels, "Optomechanical device actuation through the optical gradient force," *Nat. Photon.*, vol. 4, no. 4, pp. 211–217, Apr. 2010.
[8] M. Li, W. H. P. Pernice, C. Xiong, T. Baehr-Jones, M. Hochberg, and H. X. Tang, "Harnessing optical forces in integrated photonic circuits," *Nature*, vol. 456, no. 7221, pp. 480–485, Nov. 2008.
[9] V. R. Almeida and R. R. Panepucci, "NOEMS devices based on slot-waveguides," in *Proc. Conf. Lasers Electro-Optics/ Quant. Electron. Laser Sci. Conf.*, Baltimore, MD, 2007.
[10] K. Van Acoleyen, J. Roels, T. Claes, D. Van Thourhout, and R. Baets, "NEMS-based optical phase modulator fabricated on silicon-on-insulator," in *Proc. 8th Int. Conference GFP*, London, U.K., 2011, pp. 371–373 (FC6).
[11] Photon Design, *FIMMWAVE*, 2011. [Online]. Available: http://www.photond.com/products/fimmwave.htm
[12] ePIXfab, *The Silicon Photonics Platform*, 2011. [Online]. Available: http://www.epixfab.eu/
[13] S. K. Selvaraja, P. Jaenen, W. Bogaerts, D. Van Thourhout, P. Dumon, and R. Baets, "Fabrication of photonic wire and crystal circuits in silicon-on-insulator using 193-nm optical lithography," *J. Lightw. Technol.*, vol. 27, no. 18, pp. 4076–4083, Sep. 2009.
[14] J. Blasco and C. A. Barrios, "Compact slot-waveguide/channel-waveguide mode converter," in *Proc. Conf. Lasers Electro-Opt. Eur.*, 2005, p. 607.
[15] G. Roelkens, D. Vermeulen, D. Van Thourhout, R. Baets, S. Brision, P. Lyan, P. Gautier, and J. M. Fedeli, "High efficiency diffractive grating couplers for interfacing a single mode optical fiber with a nanophotonic silicon-on-insulator waveguide circuit," *Appl. Phys. Lett.*, vol. 92, no. 13, p. 131 101, Mar. 2008.
[16] F. R. Blom, S. Bouwstra, M. Elwenspoek, and J. H. J. Fluitman, "Dependence of the quality factor of micromachined silicon beam resonators on pressure and geometry," *J. Vac. Sci. Technol. B, Microelectron. Nanometer Struct.*, vol. 10, no. 1, pp. 19–26, Jan. 1992.